

# Wideband physical layer cognitive radio with an integrated photonic processor for blind source separation

Weipeng Zhang<sup>1\*</sup>, Alexander Tait<sup>2</sup>, Chaoran Huang<sup>3</sup>, Thomas Ferreira de Lima<sup>1,4</sup>, Simon Bilodeau<sup>1</sup>, Eric Blow<sup>1</sup>, Aashu Jha<sup>1</sup>, Bhavin J. Shastri<sup>5</sup> and Paul Prucnal<sup>1</sup>

<sup>1</sup>\*Department of Electrical and Computer Engineering, Princeton University, Princeton, 08540, New Jersey, USA.

<sup>2</sup>Department of Electrical and Computer Engineering, Queen's University, Kingston, K7L 3N6, Ontario, Canada.

<sup>3</sup>Department of Electronic Engineering, The Chinese University of Hong Kong, Hong Kong, China.

<sup>4</sup>NEC Laboratories America, Princeton, 08540, New Jersey, USA.

<sup>5</sup>Department of Physics, Engineering Physics and Astronomy, Queen's University, Kingston, K7L 3N6, Ontario, Canada.

\*Corresponding author(s). E-mail(s): [weipengz@princeton.edu](mailto:weipengz@princeton.edu);  
Contributing authors: [alex.tait@queensu.ca](mailto:alex.tait@queensu.ca);  
[crhuang@ee.cuhk.edu.hk](mailto:crhuang@ee.cuhk.edu.hk); [research@tlima.me](mailto:research@tlima.me);  
[sbilodeau@princeton.edu](mailto:sbilodeau@princeton.edu); [ecb10@princeton.edu](mailto:ecb10@princeton.edu);  
[aashuj@princeton.edu](mailto:aashuj@princeton.edu); [bhavin.shastri@queensu.ca](mailto:bhavin.shastri@queensu.ca);  
[prucnal@princeton.edu](mailto:prucnal@princeton.edu);

## Abstract

The expansion of telecommunications incurs increasingly severe crosstalk and interference, and a physical layer cognitive method, called blind source separation (BSS), can effectively address these issues. BSS requires minimal prior knowledge to recover signals from their mixtures, agnostic to carrier frequency, signal format, and channel conditions. However, the previous BSS implemented in electronics did not fulfill this versatility due to the inherently narrow bandwidth of radio-frequency (RF) components, the high energy consumption of digital signal processors (DSP), and their

shared weaknesses of low scalability. Here, we report a photonic BSS approach that inherits the advantages of optical devices and can fully fulfill its “blindness” aspect. Using a microring weight bank integrated on a photonic chip, we demonstrate energy-efficient, WDM-scalable BSS across 19.2 GHz of bandwidth, covering many standard frequency bands. Our system also has high (9-bit) accuracy for signal demixing thanks to a recently developed dithering control method, resulting in higher signal-to-interference ratios (SIR) even for ill-conditioned mixtures.

**Keywords:** Silicon Photonics, Microwave Photonics, Blind Source Separation

The limited bandwidth of conventional radio frequency (RF) equipment severely increases pressure on the RF spectrum as emerging wireless telecommunication services [1–3] are squeezed into a narrow frequency band, leading to growing spectral efficiency, the available data rate for a given bandwidth (bits/s/Hz). Many strategies have been deployed to maximize spectrum utilization, such as the multi-input and multi-output (MIMO) scheme [4–8], which enhances data-carrying capacity through space-division multiplexing. The inevitable downside incurred is degraded signal quality due to severe crosstalk among tightly packed spatial channels. Also negatively impacted are scientific services because of RF interference. Science activities, including the earth explorer services [9] (for remote sensing, satellite imagery, radar) and radio astronomy, must [10] sensitively detect noise-like signals at frequencies dictated by physical phenomena (Fig. 1). Furthermore, this increased vulnerability cannot be avoided by arbitrarily altering the frequency. One way to mitigate spectral congestion is active radio access sharing via cognitive radio [11–13], which dynamically allocates secondary users with access to the unlicensed bands that do not have primary users. However, this relies on a software-layer radio-signal identification mechanism that needs access and saves the whole spectrum, which is complicated and vulnerable to privacy breaches [14].

A physical layer cognitive technique called blind source separation (BSS) [4, 15] can extract unknown signals (e.g., a signal of interest and an interferer) from their mixtures with minimal assumptions. Operating in the physical layer allows the isolation of unwanted transmissions in the analog domain, which reduces the risk of privacy leakage by eliminating the need to record the transmission content digitally [16]. Besides, the unique “blindness” allows agility in recovering sources with arbitrary characteristics, such as frequency, modulation type, and power ratio. However, this advantage cannot be realized without BSS being performed across a wide frequency range, which can be challenging for the electronic implementations of BSS due to the limited bandwidth of conventional RF technology. Given that the spectrum of ultra-wideband (UWB) signals [17] covers up to 7.5 GHz, and that of Wi-Fi signals has expanded

from 2.4 GHz (802.11) to 6 GHz (802.11ax), to have such broadband coverage is challenging with a single RF system, as depicted in Fig. 1. In principle, using multiple subsystems designed for operating at distinct frequencies could help cover the bandwidth [18] but with prohibitively high energy cost that increases proportionally to the frequency and the unavoidable bulkiness limiting their practicality. Thus, alternative techniques other than conventional electronic processors will be required to effectively process RF signals in the next generation of wireless systems [19].

By upconverting to frequencies of hundreds of terahertz, photonic signal processors can deal with broadband information [20–22], where GHz signals are regarded as narrowband. Furthermore, photonic processing has low energy consumption that does not scale with the signal frequency. A promising on-chip processor is the microring resonator (MRR) weight bank [23, 24], a bank of tunable filters implemented with tiny circular optical waveguides, which provides energy-efficient tuning [25] and scalable parallel processing through wavelength-division-multiplexing (WDM). Such an RF frontend powered by a photonic processor (Fig. 1a) can share the workload of signal processing with a digital signal processing (DSP) backend and enhance the performance in many aspects. Nevertheless, the high tuning sensitivity of MRRs incurs vulnerability to environmental fluctuations and thermal crosstalk between adjacent MRRs. As a result, the tuning accuracy was constrained to around 7 bits [26, 27], and the related BSS performance was limited, as reflected in low signal-to-interference ratios (SIR) and large unwanted signal residuals [28]. We recently developed a dithering control method [29] that improves the tuning accuracy of MRRs beyond 9 bits.

Here, we report a photonic implementation for BSS based on the dithering-controlled MRR weight bank. We also demonstrate a fully-packaged photonic processor with a silicon photonic chip integrated with MRR driver and control electronics on a single printed circuit board (PCB). Our setup fully realizes the “blindness” agility by achieving a bandwidth of up to 19.2 GHz and SIR of more than 40 dB in some cases. Besides, the dithering weight control enables a photonic processor with 9-bit accuracy beyond many electronic counterparts, enhancing the BSS with at least one-half reduced residual error than previous trials. We also test this setup on a wireless transceiver system, proving the ability to recover a weak communication signal submerged in a wideband jamming noise, resulting in a 15 dB increase in signal-to-noise ratio. This work proves that the dithering-controlled MRR weight bank can be an up-and-coming substitute for conventional electronic BSS, bringing about unprecedented performance in many aspects, including broadband agility and higher SIR.

## BSS problem and algorithm

The BSS problem can be formulated as separating an unknown mixture of unknown independent signals. The instantaneous model of generic mixing in

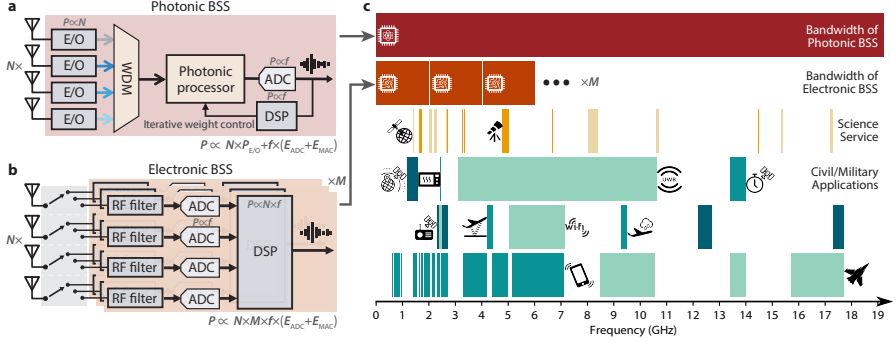


**Fig. 1 Architecture comparison between electronic and photonic BSS implementation.** **a**, Photonic BSS system diagram. **b**, Electronic BSS system diagram. **c**, Frequency allocation for common bands (from 0.5 GHz to 19 GHz) and example bandwidths for the two BSS implementations (photronics and electronics). Science service bands comprise earth explorer satellite service (EESS) and radio astronomy service (RAS). Bands for civil and military applications include global positioning system (GPS), microwave oven, ultra-wideband (UWB), and standard frequency and time signal service (for the first row); broadcasting-satellite service, radar altimeter, Wi-Fi, and aircraft weather radar (for the second row); 5G cellular networks and military radar (for the third row). In electronic BSS, covering the demanded bandwidth requires a complex switching system that consists of multiple electronic BSS setups (quantity of  $M$ ) corresponding to distinct frequency regimes. Each one requires  $N$  ADCs ( $N$  is the number of receivers) and a dedicated DSP with  $N$  inputs to perform the multiply-accumulate (MAC) operation. Since ADC and DSP require power in scale with the signal frequency, the total power consumption of the electronic BSS approaches is proportional to  $N \times M \times f \times (E_{ADC} + E_{MAC})$ . In contrast, achieving the same coverage requires only one photonic BSS setup consisting of  $N$  electrical-to-optical (E/O) converters with only one ADC and a low-end DSP with a single input. This architecture consumes much less power that is proportional to  $N \times P_{E/O} + f \times (E_{ADC} + E_{MAC})$ .

a transmission channel is  $[r_1, r_2] = \mathbf{H}[s_1, s_2]$ , where  $(s_1, s_2)$  are the source signals,  $\mathbf{H}$  is a mixing matrix representing the wireless channel, and  $(r_1, r_2)$  are the received signals. In the most general case, the source signals and their mixing matrix are unknown to the receiver. The goal of BSS is to estimate the corresponding demixing matrix,  $\mathbf{H}^{-1}$ , and apply it to the received signals to arrive at  $[s'_1, s'_2] = \mathbf{H}^{-1}[r_1, r_2]$ , where  $(s'_1, s'_2)$  is the estimated recovery of the source signals. In addition to assuming nothing about the original signals, in general, minimal prior assumptions about their characteristics can be made. For example,  $s_1$  and  $s_2$  can occupy the same frequency band, which means an implementation based on filtering would fail regardless of any receiver-side analysis. It is assumed that the two sources are statistically independent and that all mixing happened linearly. These assumptions are very realistic and are widely used in the radio community [30].

For a given mixing matrix  $\mathbf{H}$ , to retain the signal of interest and eliminate the rest, the mixtures are weighted and summed, with weights represented by each column of the inverse matrix  $\mathbf{H}^{-1}$ . A bank of tunable optical filters, an MRR weight bank as an on-chip signal processor, can perform linear weighted addition of input signals. As shown in Fig. 2a-c, the MRR weight bank consists of several microring resonators with slightly different radii; each

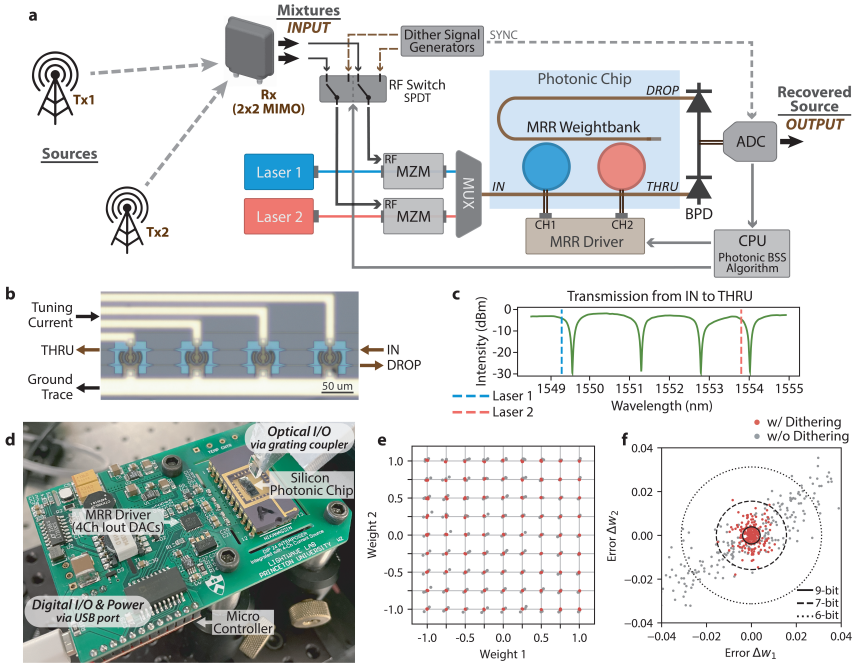


**Fig. 2 Photonic BSS experimental setup.** **a**, Schematic of the BSS setup. MZM, Mach-Zehnder modulator. MUX, wavelength-dependent multiplexer. BPD, balanced photodetector. ADC, analog to digital converter. Tx, transmitter. Rx, receiver. **b**, Micrograph of the MRR weight bank on the chip. **c**, Transmission spectrum of the THRU port at 25°C. **d**, Fully-packaged photonic processor. The silicon photonic chip, which is wire-bonded on a DIP 24 chip carrier, is mounted on the right side of this PCB. A 4-channel current output DAC is integrated on the board and applies currents for tuning the MRRs. Optical input and output (I/O) is through the grating coupler on the top right and electrical I/O is set up via a USB cable (bottom left), which also delivers the power for the whole PCB. **e**, Estimation of weighing accuracy. The 2-MRR weight bank in **a** was tested to tune the weights represented by each grid. The dithering control yielded the red points, and the gray points were obtained without the dithering. **f**, The errors of all the tested weights in **d**. A 9.0-bit of precision resulted from the dithering control and 6.7-bit for the control without the dithering.

has a Lorentzian-shaped transmission profile (as shown in Fig. 2c) centered at different wavelengths. Each MRR is equipped with a metal heater to allow thermo-optic displacement of the center wavelength by varying the current applied [31]. The MRR weight bank independently weights the laser amplitudes of different wavelengths. The sum of all optical powers can be obtained by a balanced photodetector (BPD) at the output. Utilizing this ability of weighted addition, we develop a photonic BSS algorithm, which follows a pipeline consisting of three steps, including principal component analysis (PCA) [32], whitening, and independent component analysis (ICA) (See details in Ref. [28]). Essentially, a constrained Nelder-Mead iterative algorithm [33] is carried out that performs a projection-pursuit of the mixtures to search the optimized weighting vectors. The goal is to find the mixture that outputs a weighted addition ( $\sum w_i s_i$ ,  $w_i \in [-1, 1]$ ,  $i \in [1, 2 \dots N]$ ,  $N$  is the number of the mixtures)

with maximal variance (the second-order statistic) for PCA and the maximal non-Gaussianity (the fourth-order statistic or kurtosis) for ICA.

## Photonic hardware implementation

The hardware realization of this algorithm appears as a control loop (as shown in Fig. 2a). Apart from the photonic chip, also included is a BPD for electrical-to-optical (E/O) conversion (DSC-R405ER, Discovery semiconductor), an ADC for signal digitization (DPO73304SX, Tektronix), a computer for statistical analysis and actuating weight commands, and a multi-channel current source for MRR tuning (custom-built as shown in Fig. 2d). The dithering control [29] implemented here allows control of the MRRs with less complicated drivers instead of the source-measurement unit (SMU) [26]. In this setup, the MRR driver is directly integrated into the PCB interposer, packaged close to the photonics chip with a much-reduced footprint and cable management [29]. The signal path starts from the MZM and ends at the scope, and the highest supported RF frequencies are determined by the BPD of up to 20 GHz, providing coverage for lots many commonly used RF bands. It is also worth noting that most of the signal path is in the optical domain, bringing about broadband and flat response and very low latency.

The photonic chip in this setup has a 4-channel MRR weight bank with resonance frequencies roughly spaced by 200 GHz. The spectra of the four MRRs (at 25 degrees) are shown in Fig. 2c, with the resonance peaks located at 1549.6 nm, 1551.3 nm, 1552.8 nm, and 1554.0 nm. Since this work recovers source signals from two mixtures, we use two MRRs (the leftmost and rightmost ones). The corresponding lasers (PPCL500, Pure Photonics) are tuned to be 1549.3 nm and 1553.8 nm, then amplified (FA-23, Pritel) and combined into a shared waveguide by a WDM multiplexer (MDM-15-8, Santec) before coupling into the MRR weight bank through grating couplers.

The implemented dithering control method overcomes the low accuracy incurred by the high sensitivity of the weight bank. As shown in Fig. 2a, the lasers are modulated with either the actual received mixtures or pre-defined dithering signals. Each time a set of commanded weights are applied, the RF switch (RC-2SPDT-A26, DC - 26.5 GHz, Mini-Circuits) passes the dithering signals into the photonic path, which helps adjust the driving currents of the MRRs until the output weights reach the demanded values. Then, the actual mixtures are switched into the weight bank and processed. Fig. 2e-f illustrates the weighting accuracy, which shows the resulted weights (red dots) of the two MRRs being examined at the tested values represented by each grid point. The gray dots correspond to the same targeted weight without dithering control. An improvement of over 2 bits (from 6.7 to 9 bits) is observed, enabling the MRR weight bank to have competitive performance with its electronic counterparts.

While our setup included the demonstration of the wireless transceiver system, we also had a versatile control setup that provided flexibility and accuracy in controlling the carrier frequencies and the mixing matrix. In the control

setup, the signal mixtures were generated by a high-speed multi-channel arbitrary waveform generator (N8196A, 92GSPS, Keysight) and sent to each MZM directly. The generation of the two baseband signals, the up-conversion, and the signal mixing, is performed via software tools (Python). The mixed signals are then transmitted to the photonic system.

## Theoretical impact of weighting accuracy

BSS must be able to deal with mixtures that are difficult to separate. Denoting the  $j$ th signal component in the  $i$ th mixture as  $y_{ij}(t)$ , the signal-to-interference ratio (SIR) [15] defined as

$$\mathbf{SIR}_i(\text{dB}) = 10 \log_{10} \frac{\|y_{ij'}(t)\|^2}{\sum_{j \neq j'} \|y_{ij}(t)\|^2} \quad (1)$$

is a ratio of the signal power ( $\|y_{ij'}(t)\|^2$ ) to the rest interference power ( $\sum_{j \neq j'} \|y_{ij}(t)\|^2$ ) of the  $i$ th mixture. Given a problem with  $N$  mixtures containing  $N$  sources to be separated, an often used merit is the overall SIR, which is the average of the SIR of every mixture ( $\frac{1}{N} \sum_i \mathbf{SIR}_i, i = 1, 2, \dots, N$ ). The SIR merit captures the accuracy of the system, and it can also be stated as a function of frequency, bandwidth, or other metrics. A higher SIR means better suppression of the interference signals. This metric of SIR can be extended to any mixing  $\mathbf{H}$  through the ill-condition number,  $\kappa(\mathbf{H})$  [34], defined as

$$\kappa(\mathbf{H}) = \|\mathbf{H}\| \cdot \|\mathbf{H}^{-1}\|. \quad (2)$$

This describes the demixing difficulty calculated by the mixing matrix  $\mathbf{H}$ . Mixtures with a small ill-condition number are easier to solve. Conversely, problems with a sizeable ill-condition number are challenging and prone to smaller SIR. Typically, an ill-conditioned BSS problem requires the weighting to represent the inverse matrix accurately.

$$\mathbf{H}^{-1} = \frac{a}{2a-1} \begin{bmatrix} 1 & (a-1)/a \\ (a-1)/a & 1 \end{bmatrix} \quad (3)$$

To prove this, consider a simple case where the mixing matrix is symmetrical such that  $\mathbf{H} = [[a, 1-a], [1-a, a]], a \in [0.5, 1]$ , which is often the case when two receiver antennas and the two transmitter sources are symmetrically positioned and have identical power. The inverse of matrix  $\mathbf{H}$  is given in Eq. 3. To maximize the output signal amplitudes and introduce the weighting error, Eq. 4 describes the actual matrix of mixtures that is input to the photonic BSS. This matrix is also scaled up for the maximal output weight,  $w = 1$ .  $\delta$  denotes the weight error caused by the inaccurate MRR control.

$$\mathbf{H}^{-1} = \begin{bmatrix} 1 + \delta & (a-1)/a + \delta \\ (a-1)/a + \delta & 1 + \delta \end{bmatrix} \quad (4)$$

The coefficients (proportional to the amplitudes of each source signal) of the separated results can then be expressed by Eq. 5; the percentage of error

(ignoring the noise) that remains in the recovered results can be represented as  $a\delta/(2a + 2a\delta - 1)$ . Thus, if  $a = 0.9$  as given in this problem, the control accuracy improvement from 6.7 bits ( $\delta \approx 0.019$ ) to 9 bits ( $\delta \approx 0.004$ ) could, in theory, lower the error by a factor of 4.6 (from 2.0% to 0.44%). With these equations, we can also derive that if 2% error ( $\text{SIR} \approx 33$ ) is demanded, this 2.3-bit improvement in control accuracy increases the solvable ill-condition number from 2.05 ( $a = 0.9$ ) to 10 ( $a = 0.55$ ).

$$\begin{aligned} [s'_1, s'_2] &= \mathbf{H}'^{-1}[r_1, r_2]^T = \mathbf{H}'^{-1}\mathbf{H}[s_1, s_2]^T \\ &= \begin{bmatrix} (2a-1)/a + \delta & \delta \\ \delta & (2a-1)/a + \delta \end{bmatrix} \begin{bmatrix} s_1 \\ s_2 \end{bmatrix} \end{aligned} \quad (5)$$

## Test on ill-conditioned mixing

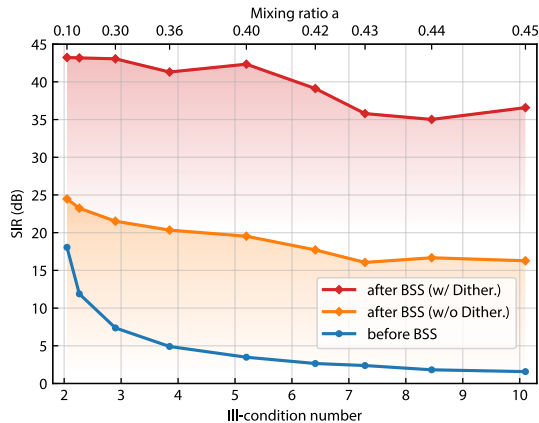


**Fig. 3 BSS performance on ill-conditioned mixtures.** Blue, red, and orange curves are the SIR before the BSS, after BSS with dithering control, and after BSS without dithering control, respectively. The mixing matrix  $\mathbf{H}$  is defined by the mixing ratio  $a$  by  $\mathbf{H} = [[a, 1 - a], [1 - a, a]]$ . The corresponding ill-condition number is calculated by Eq. 2.

Based on the setup described above, we examined the proposed photonic BSS system under different scenarios, with different signal mixtures enabled by programming the AWG. The original two signals are repeating patterns of 16 bits, and are in format of binary phase-shift keying (BPSK; bit pattern =  $[0, 1, 0, 1, 0, 1, 0, 1, 0, 1, 0, 1, 0, 1]$ ) and on-off keying (OOK; bit pattern =  $[0, 0, 1, 0, 0, 0, 1, 0, 0, 1, 0, 0, 0, 1, 0, 0]$ ), respectively. This configuration provided two short data periods that can be easily illustrated and also contributed all the potential bits combinations in their mixtures for a complete examination. Firstly, we investigated the performance of the proposed photonic BSS system in solving problems with different ill-condition numbers, which is to justify the significance of the improved weighting accuracy. Here,

we fixed the carrier frequency at 1 GHz. The mixing matrix is of symmetrical form ( $\mathbf{H} = [[a, 1 - a], [1 - a, a]]$ ) where  $a$  is varied from 0.1 to 0.45, resulting in ill-condition numbers ranging from 2.05 to 10.1. Fig. 3 shows the SIR of the mixtures obtained from the same setup but with the dithering control (compared to the previous control method without the dithering). Even in the presence of similar experimental noise levels, lower SIR is always obtained when not using dithering control. Conversely, the dithering controlled setup maintained constantly high SIR such that the influence of ill-conditioning was less distinguishable. The average SIR is above 35 dB for all tested cases, which generally shows around 20 dB improvement compared to the previous control method (the orange curve in Fig. 3). This improvement confirms the significance of accurate weight control for MRR-based applications, such as the BSS in this paper.

## Wideband capability

Next, we test the wideband capability by performing BSS on mixtures of signals from 1 GHz to 19.2 GHz by varying the carrier frequencies, as shown in Fig. 4. The baseband frequencies were also adjusted according to the carrier frequencies, which were 160 MHz for less than 1 GHz, 400 MHz for 1 - 3 GHz, 800 MHz for 3 - 6 GHz, and 1600 MHz for  $f_{\text{carrier}} \geq 4.8\text{GHz}$ . Annotating the two mixtures with M1 and M2 and the two sources with S1 and S2, the mixing can be expressed as  $M1 = 0.8 \times S1 + 0.2 \times S2$  and  $M2 = 0.2 \times S1 + 0.8 \times S2$ , denoting an ill-condition number of 2.26 (according to Eq. 2).

As shown in Fig. 4, the 22 tested frequencies from 1 GHz to 19.2 GHz show SIR of no less than 30dB. Compared with previous photonic demonstration [28] that dealt with problems of a similar ill-condition number, we obtained almost 55 times broader bandwidth (19.2 GHz versus previously 350 MHz centered at 900 MHz) while maintaining a clean signal separation across the entire band (SIR >30 vs. previously SIR $\approx$ 14). This improvement in error suppression confirms the benefit of the improved dithering control method. Also, based on the Federal Communications Commission (FCC) frequency allocation chart (partly shown in Fig. 1c), this broadband coverage by a single silicon photonic chip translates into the agility of processing multiple commonly used bands. Examples of included bands are cellular (620 MHz - 6.425 GHz), Wi-Fi (2.4 GHz, 5 - 7.125 GHz), military radar (extensive spectral usage above 8.5 GHz), and those for earth explorer satellite and radio astronomy (sparsely spread from 1.4 - 17.3 GHz). This wide bandwidth can also provide full coverage to some challenging bands, such as the ultra-wideband (UWB; 3.1 - 10.6 GHz). We also note that since signals remain narrowband at higher frequencies for photonic devices and the state-of-the-art BPD can be 100 GHz or more [35], this system can easily expand the coverage to other important spectrums like millimeter-wave just by using higher bandwidth photodetectors. The practical device footprint on-chip is  $0.13\text{ mm} \times 0.42\text{ mm}$  including four MRRs and the waveguide routing, which slowly scales up in a linear fashion with the number of sources.

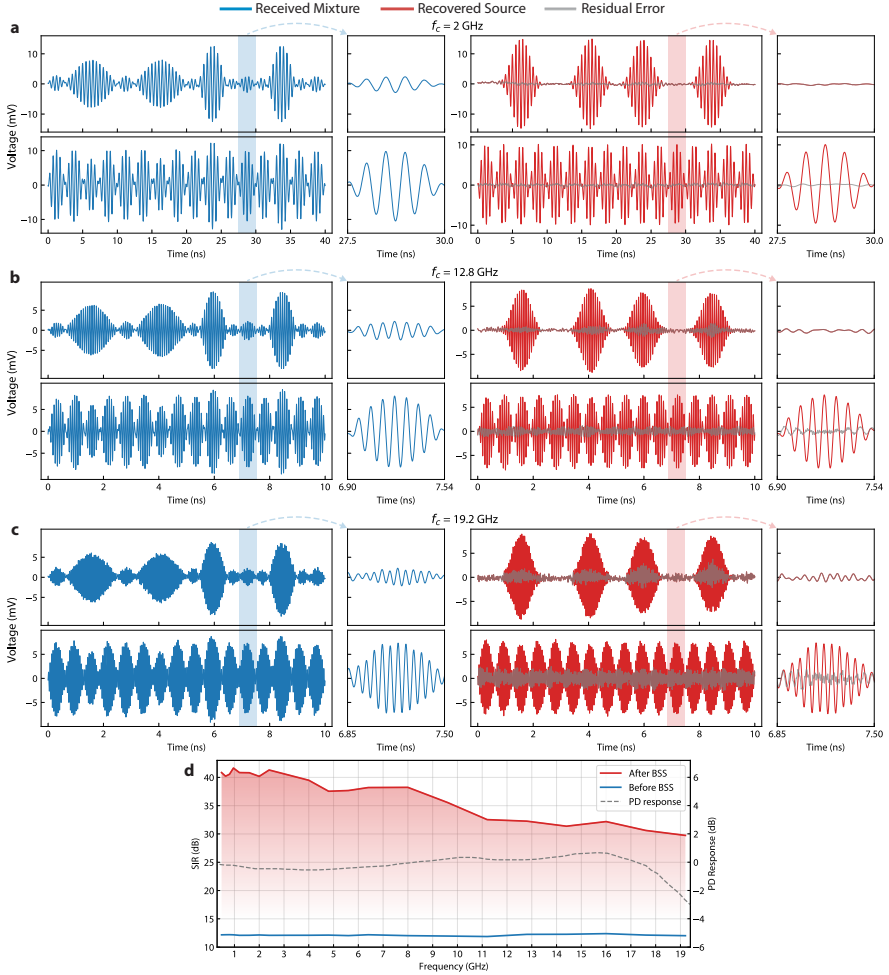


**Fig. 4 Broadband BSS with a single photonic chip.** a-c, BSS results, the mixtures and estimated sources with carrier frequencies of 2 GHz, 12.8 GHz, and 19.2 GHz, respectively. d, The SIR of the received mixtures (blue curve) and the recovered sources (red curve) versus the carrier frequency. The dashed gray curve is the relative power response of the photodetector.

## Demonstration on wireless transceiver

Next, we demonstrated our proposed BSS photonic processor in a wireless transceiver system, which emulates the case where a communication link is deteriorated by nearby RF interference. As shown in Fig. 5i, two antennas (1009-002, 1.7-2.5 GHz, Southwest Antennas) transmit the signal of interest and a broadband jammer mixed over the air with a transmission distance of 0.75 m. Then, the mixtures are received by a 2x2 MIMO antenna (1055-368, 1.7 - 2.5 GHz, Southwest Antennas), with two outputs corresponding to the polarization of 45-degree slant left and 45-degree slant right. The transmitted

signal carries a repeating sequence of 200-random bits at a baud rate of 50 MHz with a binary phase-shift keying (BPSK) modulation format and a carrier frequency of 2.1 GHz. The interference is an instantaneous wideband jamming signal generated by adding 10,000 single tones with random phases and has a spectrum from 1.7 GHz to 2.5 GHz, covering the entire bandwidth of the antennas. Thus, extracting the signal of interest is insignificantly effective via spectral filtering even if the carrier frequency is known. If doable, the signal-to-noise ratio remained the same with the received mixtures at best. In contrast, photonic BSS can recover the communication link with no prior assumptions and suppress the interference noise. Fig. 5a-h illustrates the spectrum and the constellation diagram before and after the BSS process. The signal-to-noise ratio has almost 15 dB improvement (20.8 dB to 35.5 dB), accompanied by a 2-fold increase of the Q value (5.84 to 12.6) from the constellation. This result demonstrated effective suppression of the nearby interference with high power and broad bandwidth, maintaining the transmission quality of the wireless communication link.

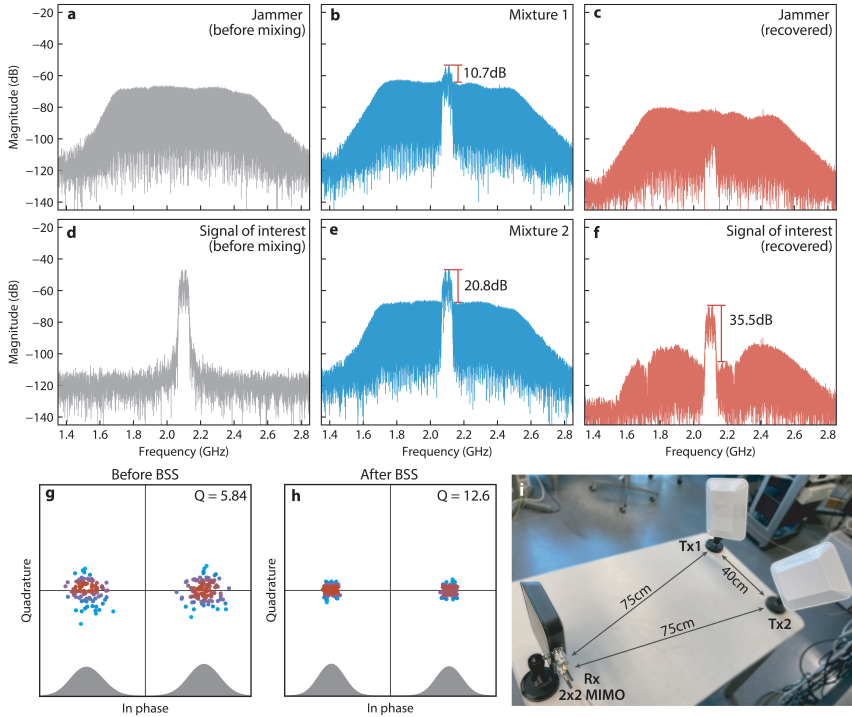


**Fig. 5 BSS demonstration on wireless transceiver system.** a, d, Spectrum of the source (Tx1) and the jammer (Tx2). These were measured at the receiver when one of the two transmitters (Tx1 or Tx2) was tuned off. b, e, Spectrum of received mixtures. c, Spectrum of the separated jamming noise. f Spectrum of the recovered source. g, h, Constellation diagram of received mixture (g, also corresponding to (e)) and recovered source (h). The Q values are 1.90 and 5.84 for the mixtures corresponding to b and e, respectively. i, Antenna setup.

## Conclusion

In summary, we explored a photonic BSS approach with an unprecedentedly high bandwidth of up to 19.2 GHz that can fully demonstrate the capability of the BSS technique. In addition, the high SIR observed for all the frequencies and ill-conditioned problems, together with an example of a wireless transceiver system, confirms that the improved MRR control method benefits the real-world applications of MRR weight banks. Overall, this work illustrates that photonic approaches are approaching readiness to replace the conventional RF implementations, effectively addressing bandwidth limitations, energy efficiency, and latency. With the incoming availability of higher speed modulators [36] and photodetectors [35] on the silicon platform, as well the maturity of packaging, including photonic wire bonding [37], laser integration [38], co-packaging of silicon and CMOS chips, and monolithic cointegration of CMOS and silicon photonics [39], this proposed photonic BSS can have future implementations with higher integration and broader bandwidth. With these, we envision a standalone BSS device of a small form factor that is field-deployable for various applications.

## Methods

### Photonic BSS algorithm

The photonic BSS algorithm follows a pipeline including principal component analysis (PCA), whitening, and independent component analysis (ICA). Firstly, photonic PCA updates the MRR weights to converge at the target PC vectors by maximizing the variance of weighted addition output  $E(y_i^2)$ . The obtained PC vectors and variances can construct a whitening matrix, which in the following step can reduce the BSS problem to finding an orthogonal transformation (rather than the inverse matrix of a mixing matrix). Then, photonic ICA utilizes this whitening matrix  $V$  and updates the MRR weight vector in the whitened subspace  $w_i V (i = 1, \dots, n)$  to converge at the target IC vectors by maximizing the absolute relative kurtosis of the output, calculated as  $|E(y_i^4)/\sigma^4(y_i) - 3|$  ( $\sigma^2$  is variance). This algorithm is inspired by the central limit theorem that the sources are supposed to maximize their non-Gaussianity (relative distance from the Gaussian distribution). Our BSS pipeline does not require explicit waveform digitization but only the second-order and fourth-order statistics of weighted addition output, unlike conventional BSS solutions like FastICA. This feature permits a low-cost ADC and DSP working at the sub-Nyquist sampling regime, generally more applicable to wideband BSS.

### Fully packaged photonic processor

We fully packaged the silicon photonic chip with its driver and control circuitry in the same interposer PCB in our experimental setup, as shown in Fig. 2d. This integration benefits a simplified lab setup, lower power consumption ( $<100$  mW), and neat connectivity that a single USB cable handles both the digital

interface and the power delivery. In terms of power management, the 5 V input (from USB cable) generates isolated and low-noise power rails by several dedicated power management ICs (LT1533CS and two LT3042, Analog Devices). These rails power up the precision current sources (LTC2662-16, 16-bit, Analog Devices), which drive the MRRs on the photonic chip. The digital interface between the current source and the controller (Arduino Pro Micro, Sparkfun) is built on the SPI protocol and isolated by a dedicated IC (ADUM4151, Analog device). This fully isolated MRR driving circuitry helps with noise suppression. Host PC commands the weights through serial communication via the USB cable. The onboard controller phrases the received command and talks to the current sources to adjust the current of each microring.

## Device fabrication

The silicon photonic chip was fabricated on a silicon-on-insulator wafer with a silicon thickness of 220 nm and a buried oxide thickness of 2  $\mu\text{m}$ . The waveguide is 500 nm wide. The weight bank consists of four MRRs (radius around  $r = 22 \mu\text{m}$ ) coupled with two bus waveguides in an add/drop configuration, and two among the four were used in the experiments. A slight difference ( $\Delta r = 0.32 \mu\text{m}$ ) was introduced in the ring radii to avoid resonance collision. The gap between the ring and bus waveguide is 200 nm, yielding a Q factor of about 6,000. Circular metal heaters were built on top of each MRR for thermally weight tuning. Metal vias and traces were deposited to connect the heater contacts of the MRR weight bank to electrical metal pads.

## Data Availability

All data used in this study are available from the corresponding authors upon reasonable request

## Code Availability

All codes used in this study are available from the corresponding authors upon reasonable request.

## References

- [1] Navarro-Ortiz, J., Romero-Diaz, P., Sendra, S., Ameigeiras, P., Ramos-Munoz, J.J., Lopez-Soler, J.M.: A survey on 5g usage scenarios and traffic models. *IEEE Communications Surveys & Tutorials* **22**(2), 905–929 (2020)
- [2] Dang, S., Amin, O., Shihada, B., Alouini, M.-S.: What should 6g be? *Nature Electronics* **3**(1), 20–29 (2020)

- [3] Saad, W., Bennis, M., Chen, M.: A vision of 6g wireless systems: Applications, trends, technologies, and open research problems. *IEEE Network* **34**(3), 134–142 (2020). <https://doi.org/10.1109/MNET.001.1900287>
- [4] Venkateswaran, V., van der Veen, A.-J.: Analog beamforming in mimo communications with phase shift networks and online channel estimation. *IEEE Transactions on Signal Processing* **58**(8), 4131–4143 (2010)
- [5] Larsson, E.G., Edfors, O., Tufvesson, F., Marzetta, T.L.: Massive mimo for next generation wireless systems. *IEEE communications magazine* **52**(2), 186–195 (2014)
- [6] Kutty, S., Sen, D.: Beamforming for millimeter wave communications: An inclusive survey. *IEEE communications surveys & tutorials* **18**(2), 949–973 (2015)
- [7] Han, S., Chih-Lin, I., Xu, Z., Rowell, C.: Large-scale antenna systems with hybrid analog and digital beamforming for millimeter wave 5g. *IEEE Communications Magazine* **53**(1), 186–194 (2015)
- [8] Ghauch, H., Kim, T., Bengtsson, M., Skoglund, M.: Subspace estimation and decomposition for large millimeter-wave mimo systems. *IEEE Journal of Selected Topics in Signal Processing* **10**(3), 528–542 (2016)
- [9] Maeda, K.: Present and future of allocation and protection of earth observation using constellation. In: 2012 IEEE International Geoscience and Remote Sensing Symposium, pp. 1073–1076 (2012). IEEE
- [10] Burke, B.F., Graham-Smith, F., Wilkinson, P.N.: *An Introduction to Radio Astronomy*. Cambridge University Press, Cambridge (2019)
- [11] Haykin, S.: Cognitive radio: brain-empowered wireless communications. *IEEE journal on selected areas in communications* **23**(2), 201–220 (2005)
- [12] Akyildiz, I.F., Lee, W.-Y., Vuran, M.C., Mohanty, S.: Next generation/-dynamic spectrum access/cognitive radio wireless networks: A survey. *Computer networks* **50**(13), 2127–2159 (2006)
- [13] Akyildiz, I.F., Lee, W.-Y., Vuran, M.C., Mohanty, S.: A survey on spectrum management in cognitive radio networks. *IEEE Communications magazine* **46**(4), 40–48 (2008)
- [14] Fragkiadakis, A.G., Tragos, E.Z., Askoxylakis, I.G.: A survey on security threats and detection techniques in cognitive radio networks. *IEEE Communications Surveys & Tutorials* **15**(1), 428–445 (2012)

- [15] Choi, S., Cichocki, A., Park, H.-M., Lee, S.-Y.: Blind source separation and independent component analysis: A review. *Neural Information Processing-Letters and Reviews* **6**(1), 1–57 (2005)
- [16] Tait, A.N., De Lima, T.F., Ma, P.Y., Chang, M.P., Nahmias, M.A., Shastri, B.J., Mittal, P., Prucnal, P.R.: Blind source separation in the physical layer. In: 2018 52nd Annual Conference on Information Sciences and Systems (ciss), pp. 1–6 (2018). IEEE
- [17] Yang, L., Giannakis, G.B.: Ultra-wideband communications: an idea whose time has come. *IEEE Signal Processing Magazine* **21**(6), 26–54 (2004). <https://doi.org/10.1109/MSP.2004.1359140>
- [18] Solutions, I.S.: Choosing the right rf switches for smart mobile device applications. Skyworks Solutions, Inc., Tech. Rep (2011)
- [19] Lin, X.: Artificial intelligence built on wireless signals. *Nature Electronics* **5**(2), 69–70 (2022)
- [20] Marpaung, D., Yao, J., Capmany, J.: Integrated microwave photonics. *Nature photonics* **13**(2), 80–90 (2019)
- [21] Shastri, B.J., Tait, A.N., Ferreira de Lima, T., Pernice, W.H., Bhaskaran, H., Wright, C.D., Prucnal, P.R.: Photonics for artificial intelligence and neuromorphic computing. *Nature Photonics* **15**(2), 102–114 (2021)
- [22] Huang, C., Fujisawa, S., de Lima, T.F., Tait, A.N., Blow, E.C., Tian, Y., Bilodeau, S., Jha, A., Yaman, F., Peng, H.-T., *et al.*: A silicon photonic–electronic neural network for fibre nonlinearity compensation. *Nature Electronics* **4**(11), 837–844 (2021)
- [23] Tait, A.N., Wu, A.X., de Lima, T.F., Zhou, E., Shastri, B.J., Nahmias, M.A., Prucnal, P.R.: Microring weight banks. *IEEE Journal of Selected Topics in Quantum Electronics* **22**(6), 312–325 (2016). <https://doi.org/10.1109/JSTQE.2016.2573583>
- [24] de Lima, T.F., Doris, E.A., Bilodeau, S., Zhang, W., Jha, A., Peng, H.-T., Blow, E.C., Huang, C., Tait, A.N., Shastri, B.J., *et al.*: Design automation of photonic resonator weights. *Nanophotonics* (2022)
- [25] Tait, A.N.: Quantifying power in silicon photonic neural networks. *Phys. Rev. Applied* **17**, 054029 (2022). <https://doi.org/10.1103/PhysRevApplied.17.054029>
- [26] Tait, A.N., Jayatileka, H., Lima, T.F.D., Ma, P.Y., Nahmias, M.A., Shastri, B.J., Shekhar, S., Chrostowski, L., Prucnal, P.R.: Feedback control for microring weight banks. *Opt. Express* **26**(20), 26422–26443 (2018).

<https://doi.org/10.1364/OE.26.026422>

- [27] Huang, C., Bilodeau, S., Ferreira de Lima, T., Tait, A.N., Ma, P.Y., Blow, E.C., Jha, A., Peng, H.-T., Shastri, B.J., Prucnal, P.R.: Demonstration of scalable microring weight bank control for large-scale photonic integrated circuits. *APL Photonics* **5**(4), 040803 (2020)
- [28] Ma, P.Y., Tait, A.N., Zhang, W., Karahan, E.A., de Lima, T.F., Huang, C., Shastri, B.J., Prucnal, P.R.: Blind source separation with integrated photonics and reduced dimensional statistics. *Opt. Lett.* **45**(23), 6494–6497 (2020). <https://doi.org/10.1364/OL.409474>
- [29] Zhang, W., Huang, C., Peng, H.-T., Bilodeau, S., Jha, A., Blow, E., de Lima, T.F., Shastri, B.J., Prucnal, P.: Silicon microring synapses enable photonic deep learning beyond 9-bit precision. *Optica* **9**(5), 579–584 (2022)
- [30] Fabrizio, G., Farina, A.: Blind source separation with the generalised estimation of multipath signals algorithm. *IET Radar, Sonar & Navigation* **8**(9), 1255–1266 (2014)
- [31] Tait, A.N., de Lima, T.F., Nahmias, M.A., Shastri, B.J., Prucnal, P.R.: Multi-channel control for microring weight banks. *Opt. Express* **24**(8), 8895–8906 (2016). <https://doi.org/10.1364/OE.24.008895>
- [32] Ma, P.Y., Tait, A.N., de Lima, T.F., Abbaslou, S., Shastri, B.J., Prucnal, P.R.: Photonic principal component analysis using an on-chip microring weight bank. *Opt. Express* **27**(13), 18329–18342 (2019). <https://doi.org/10.1364/OE.27.018329>
- [33] Hyvärinen, A., Oja, E.: Independent component analysis: algorithms and applications. *Neural Networks* **13**(4), 411–430 (2000). [https://doi.org/10.1016/S0893-6080\(00\)00026-5](https://doi.org/10.1016/S0893-6080(00)00026-5)
- [34] Belsley, D.A., Kuh, E., Welsch, R.E.: *Regression Diagnostics: Identifying Influential Data and Sources of Collinearity*, pp. 100–104. John Wiley & Sons, New Jersey (2005). Chap. The Condition Number
- [35] Lischke, S., Peczek, A., Morgan, J., Sun, K., Steckler, D., Yamamoto, Y., Korndörfer, F., Mai, C., Marschmeyer, S., Fraschke, M., *et al.*: Ultra-fast germanium photodiode with 3-db bandwidth of 265 ghz. *Nature Photonics* **15**(12), 925–931 (2021)
- [36] He, M., Xu, M., Ren, Y., Jian, J., Ruan, Z., Xu, Y., Gao, S., Sun, S., Wen, X., Zhou, L., *et al.*: High-performance hybrid silicon and lithium niobate mach-zehnder modulators for 100 gbit s<sup>-1</sup> and beyond. *Nature Photonics* **13**(5), 359–364 (2019)

- [37] Lindenmann, N., Balthasar, G., Hillerkuss, D., Schmogrow, R., Jordan, M., Leuthold, J., Freude, W., Koos, C.: Photonic wire bonding: a novel concept for chip-scale interconnects. *Optics express* **20**(16), 17667–17677 (2012)
- [38] Zhou, Z., Yin, B., Michel, J.: On-chip light sources for silicon photonics. *Light: Science & Applications* **4**(11), 358–358 (2015)
- [39] Giewont, K., Nummy, K., Anderson, F.A., Ayala, J., Barwicz, T., Bian, Y., Dezfulian, K.K., Gill, D.M., Houghton, T., Hu, S., Peng, B., Rakowski, M., Rauch, S., Rosenberg, J.C., Sahin, A., Stobert, I., Stricker, A.: 300-mm monolithic silicon photonics foundry technology. *IEEE Journal of Selected Topics in Quantum Electronics* **25**(5), 1–11 (2019). <https://doi.org/10.1109/JSTQE.2019.2908790>

## Acknowledgments

This research is supported by the National Science Foundation (NSF) (ECCS-2128608 and ECCS-1642962), the Office of Naval Research (ONR) (N00014-18-1-2297 and N00014-20-1-2664), and the Defense Advanced Research Projects Agency (HR00111990049). The devices were fabricated at the Advanced Micro Foundry (AMF) in Singapore through the support of CMC Microsystems. B. J. Shastri acknowledges support from the Natural Sciences and Engineering Research Council of Canada (NSERC). S. Bilodeau acknowledges funding from the Fonds de recherche du Québec - Nature et technologies.

## Author contributions

W.Z., T.F.L. and A.T. conceived the ideas and implemented the experimental setup, designed the experiment, conducted the experimental measurements and analysed the results. T.F.L., E.C.B., S.B. and A.J. designed the silicon photonic chip. T.F.L, C.H., A.T. and B.J.S. provided the theoretical support. E.C.B. and S.B. performed the chip packaging. W.Z., A.T., C.H., S.B. and B.J.S. wrote the manuscript. P.R.P. supervised the research and contributed to the general concept and interpretation of the results. All the authors discussed the data and contributed to the manuscript.

## Competing interests

The authors declare no competing interests.